Evidence for the Proximity of Calcium to the Manganese Cluster of Photosystem II: Determination by X-ray Absorption Spectroscopy†

Matthew J. Latimer,[‡,§] Victoria J. DeRose,[‡,§,||] Ishita Mukerji,[‡,§,⊥] Vittal K. Yachandra,*[,§] Kenneth Sauer,*[,‡,§] and Melvin P. Klein*[,§]

Structural Biology Division, Lawrence Berkeley Laboratory, and Department of Chemistry, University of California, Berkeley, California 94720

Received May 3, 1995; Revised Manuscript Received June 15, 1995[⊗]

ABSTRACT: The photosynthetic oxygen-evolving complex contains a cluster of four manganese atoms and requires both Ca and Cl for activity. The question of Ca proximity to the Mn cluster has been investigated by performing Mn X-ray absorption experiments on native samples of photosystem II (PS II) and on samples depleted of Ca and reconstituted by either Ca or Sr. Analysis of X-ray K-edge spectra demonstrates no significant differences in oxidation state or symmetry between Ca- and Sr-reactivated preparations. Differences are observed in the extended X-ray absorption fine structure (EXAFS). The amplitude of a Fourier transform peak due to scatterers at distances greater than 3 Å is larger for samples reactivated with strontium than for calcium-reactivated samples. Taking into account the stoichiometry of Mn and Ca atoms in PS II, and considering physically reasonable structures, curve-fitting analyses of the EXAFS data using FEFF5-calculated parameters favor a model where both manganese and calcium (or strontium) scatterers contribute to the Fourier peak at approximately 3 Å. Other models for the ~3 Å peak with multiple Mn−Mn interactions or multiple Mn−Ca(Sr) interactions can also be fit to the data, but are considered less likely. This result provides confirmation for the structural proximity of Ca to the Mn cluster suggested previously [Yachandra, V. K., et al. (1993) *Science 260,* 675−679]. Possible structural arrangements for a calcium-binding site are discussed.

Photosynthetic oxygen evolution is a light-driven process carried out by the photosystem II (PS II)[1] reaction center found in plants and cyanobacteria. Single-electron photooxidations of a specialized chlorophyll molecule in the reaction center in PS II are coupled to the four-electron oxidation of water by the oxygen-evolving complex (OEC) in PS II. The OEC cycles through five states labeled S_0−S_4, where absorption of light in the reaction center drives transitions through the S_0−S_4 sequence, and S_4 spontaneously decays to S_0 with the release of dioxygen (Kok et al., 1970). A protein-bound complex of four manganese atoms is thought to be the site of water oxidation chemistry and to function in charge accumulation, storing oxidizing equivalents until the water oxidation reaction can occur. Although the manganese complex in PS II has been the subject of numerous biochemical and spectroscopic studies, the exact structure of the complex and the mechanism of water oxidation remain unknown [for recent reviews of the OEC, see Debus (1992), Rutherford et al. (1992), Sauer et al. (1992), and Wieghardt (1994)].

Calcium has been shown (in addition to manganese and chloride) to be an essential cofactor in oxygen evolution [reviewed in Yocum (1991) and Debus (1992)]. Most commonly, treatments with high NaCl concentrations (1.2 M) or with a low-pH (3.0)/citrate incubation have been employed to deplete calcium from PS II. These treatments produce preparations in which oxygen evolution is inhibited, but can be reactivated by the addition of Ca^{2+}. Partial reactivation of oxygen evolution in inhibited preparations can also be achieved by the addition of Sr^{2+} (Ghanotakis et al., 1984) or vanadyl ions (VO^{2+}) (Lockett et al., 1990). Although many other metal ions have been shown to compete with Ca^{2+} for binding sites in PS II (Na^+, K^+, Cd^{2+}, and various lanthanides), none of them results in the reactivation of oxygen evolution activity (Yocum, 1991; Debus, 1992).

Addition of Sr^{2+} to calcium-depleted preparations has been shown to reactivate the same number of centers as Ca^{2+}, but with slower turnover in the S-state cycle, producing a lower overall rate of oxygen evolution at saturating light intensities (Boussac & Rutherford, 1988a). Reactivation with Sr^{2+} also produces an altered manganese complex, as evidenced by changes in the S_2-state multiline EPR signal (Boussac & Rutherford, 1988a,b). The multiline signal produced in Sr^{2+}-reactivated preparations has a narrower average line spacing (~71 vs ~88 G in untreated preparations) and a different pattern of intensities compared to the normal multiline signal from untreated PS II preparations.

The stoichiometry of Ca^{2+} in PS II has been a matter of some confusion, although most results seem to point to there

† This research was supported by the Director, Office of Basic Energy Sciences, Division of Energy Biosciences, of the U.S. Department of Energy under Contract No. DE-AC03-76SF00098 and by a grant from the National Science Foundation (DMB91-04104).

* Authors to whom correspondence should be addressed.

‡ Department of Chemistry.

§ Structural Biology Division.

|| Present address: Department of Chemistry, Northwestern University, Evanston, IL 60208.

⊥ Present address: Department of Molecular Biology and Biochemistry, Wesleyan University, Middletown, CT 06459-0175.

⊗ Abstract published in *Advance ACS Abstracts,* August 1, 1995.

[1] Abbreviations: Chl, chlorophyll; DCBQ, 2,5-dichloro-*p*-benzoquinone; DMSO, dimethyl sulfoxide; EPR, electron paramagnetic resonance; EXAFS, extended X-ray absorption fine structure; EGTA, ethylene glycol bis(β-aminoethyl ether)-*N,N,N′,N′*-tetraacetic acid; MES, (4-morpholino)ethanesulfonic acid; OEC, oxygen-evolving complex; PS II, photosystem II; XAS, X-ray absorption spectroscopy.

0006-2960/95/0434-10898$09.00/0

being two Ca^{2+} per PS II reaction center: one high-affinity binding site that requires extreme conditions for removal and a second, lower affinity site from which Ca^{2+} can be removed by the NaCl or low-pH treatments discussed earlier [for discussions of this point, see Debus (1992), Rutherford (1992), and Yocum (1991)]. For the low-pH/citrate treatment it has been specifically reported that one of the two Ca^{2+}/PS II is removed (Ono & Inoue, 1988).

The effects on the S_2-state multiline EPR signal of reactivation with Sr^{2+} and the experiments linking calcium reconstitution with the reactivation of activity in Ca-depleted preparations have fueled speculation that there is a Ca-binding site closely associated with the Mn cluster in PS II.

X-ray absorption spectroscopy (XAS) is an excellent tool for examining the immediate structural environment of metal ions in proteins. XAS has the advantage of being element-specific and does not require a crystalline sample; thus, it has proved to be a useful technique for probing the structure of the Mn complex of PS II, where many components (non-heme iron, cytochrome, etc.) normally present in active preparations can interfere with other spectroscopic techniques. X-ray absorption edges can be examined to determine the oxidation states and site symmetry of the Mn, and extended X-ray absorption fine structure (EXAFS) gives information about the radial distribution of atoms around the Mn atoms of PS II. In addition to distances, EXAFS is sensitive to the number and atomic number of atoms around the absorbing atom [for reviews of XAS in biological systems, see Scott (1985), Cramer (1988), and Yachandra (1995)].

Previous results from EXAFS on PS II preparations [reviewed in Sauer et al. (1992)] have indicated that the structure contains a Mn−Mn distance of 2.7 Å, which is a characteristic distance in di-μ-oxo-bridged Mn model complexes (Wieghardt, 1989; Pecoraro, 1992). Consistent with this result, short bonds to oxygen/nitrogen atoms of 1.8 Å have been detected, which is also characteristic of distances to bridging oxo groups in model complexes. A longer distance interaction has also been detected, but the interpretations differ. Among them are (1) a single Mn−Mn distance of 3.3 Å (George et al., 1989; DeRose et al., 1994), (2) a Mn−Mn or Mn−Ca at 3.3 Å (Penner-Hahn et al., 1990), (3) Mn−Mn and Mn−Ca at ~3.3 Å (Yachandra et al., 1993; DeRose et al., 1994), and (4) a single Mn−Ca at 3.7 Å (MacLachlan et al., 1992).

We have published possible models for the OEC based on a Mn−Mn interaction at 3.3 Å, but at the time were unable to make a full determination concerning Ca contributions at that distance (DeRose et al., 1994).

In this paper, we report the results of experiments using XAS spectroscopy to determine the effects of replacement of Ca by Sr on the structure of the Mn complex of PS II. The dominant effect is an increase in the amplitude of the third Fourier peak in the EXAFS of PS II reactivated with Sr^{2+} relative to that of PS II preparations reactivated with Ca^{2+}. Simulations of the EXAFS and structural constraints favor a model in which there are both Mn−Mn and Mn−Ca/Sr pairs contributing to the third Fourier transform peak in the EXAFS. The Mn−Ca/Sr distance is indicative of a uniquely close association of Ca and Mn. Possible structural arrangements of Ca and Mn are discussed. Portions of this work have been reported in summary form elsewhere (Yachandra et al., 1993).

MATERIALS AND METHODS

Preparation of Ca^{2+}- and Sr^{2+}-Reactivated PS II Samples. Triton X-100-extracted PS II particles were prepared from market spinach according to the procedure of Berthold et al. (1981).

Ca-depletion treatments were performed according to the low-pH/citrate procedure of Ono and Inoue (1988). Briefly, PS II particles in 0.4 M sucrose, 25 mM MES (pH 6.5), and 15 mM NaCl were pelleted by centrifugation (15 min at 40000*g*) and then resuspended to approximately 6 mg of Chl/mL in 0.4 M sucrose, 0.25 mM MES (pH 6.5), and 15 mM NaCl buffer. The particles were then diluted to 2 mg of Chl/mL in 0.4 M sucrose, 20 mM citrate (pH 3.0), and 15 mM NaCl buffer. After a 5 min incubation at 0 °C, the preparation was brought to pH 6.5 with buffer A [0.4 M sucrose, 50 mM MES (pH 6.5), 15 mM NaCl, and 100 μM EGTA] and pelleted by centrifugation (15 min at 40000*g*). The membranes were then resuspended in buffer A and pelleted again. The final step before sample preparation was resuspension in buffer B [25 mM MES (pH 6.5), 15 mM NaCl, and 100 μM EGTA] with either 50 mM $CaCl_2$ or $SrCl_2$ (for Ca-PS II and Sr-PS II samples) or no addition (for Ca-depleted samples). The resuspensions with $CaCl_2$ and $SrCl_2$ were performed under ambient light and were homogenized slowly by hand to ensure uniform suspension and illumination. Ethanol has been shown to minimize the $g = 4.1$ EPR signal in PS II preparations from spinach (Zimmermann & Rutherford, 1986), and we have found (data not shown) that the addition of ethanol also suppresses the $g = 4$ EPR signal in Sr-reactivated preparations; thus, samples were made with 2.5% ethanol (v/v) in the final resuspension step.

Finally, the treated PS II particles were again centrifuged (30 min at 40000*g*), and the resulting pellets were transferred to lucite sample holders designed to fit into both EPR and X-ray cryostats. Ca-reactivated (Ca-PS II) and Sr-reactivated (Sr-PS II) samples were allowed to dark-adapt for about 1 h on ice and then were frozen in liquid nitrogen. All samples were stored and transported in liquid nitrogen, and care was taken to prevent warming when transferring them to the liquid helium cryostats used for EPR and X-ray spectroscopy.

All glassware, centrifuge tubes, etc. were acid-washed, and all buffers used in the Ca-depletion procedure were treated with Chelex-100 (Bio-Rad) to remove any Ca contamination in the chemicals used in the buffers.

Oxygen Evolution Measurements. Oxygen evolution activity was measured by using a Clark-type oxygen evolution electrode as described by DeRose (1990). The electron acceptor DCBQ was added from a stock solution in DMSO to a final concentration of 2 mM. The oxygen evolution activity of untreated PS II particles was 500−600 μmol of O_2/mg of Chl/h. Oxygen evolution of Ca-depleted preparations was measured in buffer A (see above) with no addition or with 50 mM $CaCl_2$ or $SrCl_2$. Oxygen evolution activity was inhibited in Ca-depleted PS II to ~15% of the value measured in untreated preparations. Addition of Sr^{2+} resulted in the reactivation of oxygen evolution activity to ~40%, while the addition of Ca^{2+} reactivated activity to ~80% of that in untreated preparations. Chlorophyll assays were performed on acetone extracts following the method of Arnon (1949).

EPR Spectroscopy. Low-temperature EPR spectra were collected using a Varian E-109 EPR spectrometer equipped

with an Air Products Helitran liquid helium cryostat. All samples were characterized by low-temperature EPR prior to exposure to X-rays and were examined afterward to ensure that no damage (Mn release) had occurred due to X-ray exposure or sample handling. Ca- and Sr-reactivated samples were advanced to the S_2 state by illumination for 10 min at 195 K with a 400 W tungsten lamp, employing a 5 cm aqueous $CuSO_4$ filter (5%, w/v) for thermal isolation. A modified S_2 state was formed in Ca-depleted samples by illumination for 2 min at 0 °C, followed by incubation in darkness for 15 min at 0 °C.

X-ray Absorption Spectroscopy. Mn X-ray absorption edge spectra were collected at Stanford Synchrotron Radiation Laboratory (SSRL) on beamline IV-2 using a Si(220) double-crystal monochromator. Mn K-edge data were recorded as fluorescence excitation spectra (Jaklevic et al., 1977) using a lithium-drifted silicon solid-state detector [described in Guiles et al. (1990)]. Energy calibration (Goodin et al., 1979) and measurement of incident flux were carried out as described by Guiles et al. (1990).

EXAFS spectra were collected on beamline X-9A at the National Synchrotron Light Source, Brookhaven National Laboratory, and at SSRL on beamlines VII-3 and IV-2. All EXAFS data were collected by using a Si(220) double-crystal monochromator and a 13-element Ge detector (Cramer et al., 1988). For both Mn K-edge and EXAFS experiments, samples were maintained at 10−12 K using an Oxford Instruments CF 1208 liquid helium flow cryostat.

XAS Data Analysis. Data reduction for EXAFS and edge spectra were performed as reported previously (Guiles et al., 1990; DeRose et al., 1994). Second derivatives of Mn K-edge spectra, which accentuate the shape of the edges, were derived by analytical differentiation of a third-order polynomial fit over a ±2.5 eV range around each point.

All EXAFS spectra were converted from energy (electronvolts) to photoelectron wave vector [k-space, (angstroms)$^{-1}$)] using the equation:

$$k = (2\pi/h)[2m_e(E - E_0)]^{1/2} \quad (1)$$

where h is Planck's constant, m_e is the mass of the electron, E is the X-ray energy, and E_0 is the ionization threshold, which was chosen as 6563.0 eV for all spectra (a point near the peak of the edge). All spectra were weighted by k^3 and Fourier transforms were calculated from k-space spectra truncated to zero crossings in the data to minimize apodization distortions (≈3.6−11.2 Å^{-1}). It was found that the removal of a two-domain spline in energy space was most effective in reducing the amplitude of background peaks at R′ < 1 Å in these Fourier transforms, and the data presented here have been processed in this manner with no further background removal in k-space.

Fourier isolation is commonly used to help simplify curve fitting of EXAFS data, allowing analysis of the contribution of single peaks. The isolation process, however, can introduce distortions in the extracted k-space data, especially at the start and end of the spectrum (Teo, 1986). Closely spaced Fourier peaks can also be distorted if isolated individually. There is a tradeoff in this, however, for a small peak next to a larger one. If the peaks are isolated together, then the spectrum is dominated by the contribution from the larger peak and the structural information in the smaller peak can be difficult to extract reliably. If the peaks are isolated individually, then the isolation process could greatly distort the smaller peak, as well as the resulting curve-fitting analysis. For analysis of the data presented here, Fourier peaks were isolated individually and in pairs to help simplify the spectra and to minimize the effects of distortions due to Fourier isolation (Zhang et al., 1988). Ranges of the Fourier transforms were isolated for analysis by the application of a Hamming window function (applied to the first and last 15% of the range; the middle 70% was left unmodified) to the transform.

Curve fitting was done using *ab initio*-calculated phase and amplitude information. Both tabulated values (McKale et al., 1988) and calculated values using the program FEFF5 (version 5.05; Rehr et al., 1991, 1992) were employed. Only fit results using FEFF5-calculated parameters are presented here, although similar information was obtained from fits using the McKale tables.

The following equation was used in curve fitting of the EXAFS data:

$$\chi(k) = S_0^2 \sum_i N_i B_i(k) \frac{f_{\text{eff}}(\pi,k,R_i)}{kR_i^2} e^{-2\sigma^2 k^2} e^{-2R_i/\lambda(k)} \times \sin[2kR_i + 2\delta_i^c(k) + \phi_i(k)] \quad (2)$$

where for each shell i, N is the number of scatterers at distance R, S_0^2 is a many-body amplitude reduction factor, $B(k)$ is an amplitude reduction factor caused by inelastic losses in the central atom, $f_{\text{eff}}(\pi,k,R)$ is the effective backscattering amplitude of the scattering atom, $\delta^c(k)$ and $\phi(k)$ are phase shifts for the absorber and backscatterer, respectively, σ^2 is a Debye−Waller term, and $\lambda(k)$ is the mean-free-path of the photoelectron. Coordination numbers (N) are calculated on a per Mn basis and are interpreted here in the context of a total of four Mn atoms per PS II. This means that a single Mn−scatterer interaction in the complex would result in a coordination number of 0.25. More scatterers would appear in multiples of 0.25. In the case of Mn−Mn interactions, however, one Mn−Mn interaction would give a minimum coordination number of 0.5 since both of the Mn's would "see" each other at the same distance. More Mn−Mn interactions at the same distance would give multiples of 0.5 for the coordination number.

FEFF5 fitting parameters [$f_{\text{eff}}(\pi,k,R_i)$, $\delta^c(k)$, $\phi(k)$, $\lambda(k)$] were calculated for isolated pairs of atoms and from a simple structural model of the Mn complex, including an approximate first coordination shell around each Mn atom and containing structural elements (Mn di-μ-oxo binuclear units) known/proposed to be present in the OEC. Also included in this simple model were Mn−Mn, Mn−Ca, Mn−Sr, or Mn-C interactions (calculated for a distance range of 3.0−3.6 Å), depending on which were needed for curve fitting. Through comparisons with calculations based on model compound crystal structures, it was found that the inclusion of an approximate coordination shell around the atoms in the calculation gave more reasonable mean-free-path values than calculations using simple pairs of atoms. This in turn also gives a more reliable estimate of the disorder parameter (σ^2); thus, calculations based on the structural model were used.

The use of FEFF5-calculated parameters also allowed us to use an additional simplification, in that a single ΔE_0 value

was used in multishell fits. It was found by O'Day et al. (1994) that, in fitting the EXAFS from inorganic complexes with FEFF-calculated parameters, they were able to use the ΔE_0 value obtained from fits to the first shell in fits to higher shells and obtain correct distance information. In our case, the first peak is not fit well enough to allow a confident estimation of the ΔE_0 parameter for use in fitting longer distance interactions. We have chosen instead to limit each fit to a single ΔE_0 parameter for all shells.

The quality of the fits presented here was evaluated by using the normalized error sum, Φ, given by the equation:

$$\Phi = \sum_{i}^{N} (1/s_i^2)(\chi^{\text{exptl}}(k_i) - \chi^{\text{theor}}(k_i))^2 \quad (3)$$

where N is the number of data points and s_i is defined as

$$1/s_i = k_i^3 / \sum_{j}^{N} k_j^3 |\chi_j^{\text{exptl}}(k_j)| \quad (4)$$

The ϵ^2 error takes into account the number of variable fit parameters (p) and the number of independent data points (N_{ind}):

$$\epsilon^2 = [N_{\text{ind}}/(N_{\text{ind}} - p)]N^{-1}\Phi \quad (5)$$

The number of independent data points is estimated to be equal to $2\Delta k \Delta R/\pi$, where Δk is the k-range of the data used and ΔR is the width of the Fourier-filtered peak [for details, see Bunker et al. (1991) and Binsted et al. (1992)]. A negative value for ϵ^2 indicates that the fit is underdetermined and the fit solution is generally considered not to be unique. The ϵ^2 value allows one to distinguish whether the inclusion of additional shells in a fit (thus increasing the number of free parameters p) actually improves the quality of the fit by explicitly accounting for the degrees of freedom. A model-based approach [where certain parameters (e.g., N, σ^2) were kept fixed] was adopted for several of the multishell fits, resulting in the same (or even fewer) number of free-floating parameters as fits with fewer shells. These fits are specifically model-dependent, and this should be kept in mind when reviewing fit error parameters.

RESULTS

EPR Spectroscopy. Low-temperature EPR spectra from Ca- and Sr-reactivated samples, as well as from a Ca-depleted sample, are presented in Figure 1. Each spectrum is the difference between the spectrum after illumination (S_2 state) and the spectrum from the same dark-adapted (S_1 state) sample. The spectra displayed in Figure 1A show the g = 4 region. Ca-reactivated samples show no light-induced g = 4 signal, while Sr-reactivated samples do show a small g = 4 signal. Boussac and Rutherford (1988a,b) reported similar effects on the g = 4 region (i.e., an increased g = 4 signal) in Sr-reactivated samples that had been depleted of Ca using high concentrations of NaCl, chelators, and light. The Ca-depleted sample also shows a signal in the g = 4 region, but this is due to the disappearance of a signal present in the S_1 state. This signal has been attributed to an iron(III) citrate complex formed in less than 10% of PS II centers during the low-pH, Ca-depletion treatment and is associated with the acceptor side of PS II (Tso et al., 1991).

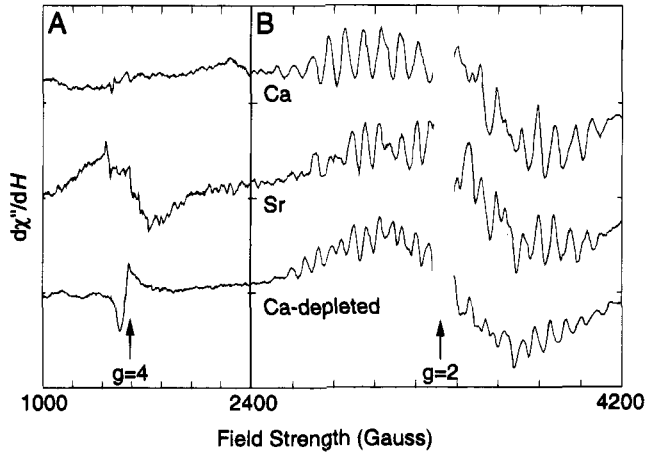

FIGURE 1: X-band EPR spectra of Ca- and Sr-reactivated PS II. Also shown is the spectrum of a Ca-depleted sample in a modified S_2 state. Spectra of the g = 4 region (A) and the g = 2 multiline region (B) are presented. Spectra are the differences between spectra from illuminated samples and spectra of the same sample prior to illumination (i.e., dark-adapted). Samples were illuminated to obtain the S_2 state as described in the text. Spectrometer conditions: microwave frequency, 9.21 GHz; microwave power, 20 mW; modulation amplitude, 20 G; temperature, 8 K. Differences between the samples in the g = 4 region are shown in (A), where Sr reactivation enhances a g = 4 signal that is not present in Ca-reactivated or Ca-depleted spectra. Mn multiline spectra are illustrated with an expanded x-axis in (B) and clearly show the reduced line spacing and different amplitude patterns in the Sr-reactivated sample vs the Ca-reactivated sample. The Ca-depleted multiline signal has more lines and smaller line spacing than do multiline signals from either Ca- or Sr-reactivated samples. The y-scales in both plots are the same, allowing direct comparison of the amplitudes of g = 4 and g = 2 signals.

Manganese multiline signals are displayed on an expanded x-scale in Figure 1B (both panels A and B are plotted on the same y-scale). The multiline signal observed in Ca-PS II is identical to that found in untreated PS II preparations, and in Sr-PS II a modified multiline signal is observed with changes in overall line spacings (~73 vs ~88 G in Ca-PS II) and intensities similar to those reported for Sr-reactivated preparations (Boussac & Rutherford, 1988a,b; Ono & Inoue, 1989). For comparison, a spectrum from a Ca-depleted sample made before Ca or Sr reactivation is presented. The Ca-depleted multiline spectrum has a greater number of resolvable lines, has an even smaller line spacing, and is stable for long periods of time in the dark at 0 °C. The conditions for its generation were the same as reported previously for these preparations (Boussac et al., 1989; Sivaraja et al., 1989). We also note that illumination of the Ca-depleted sample at 200 K induced no "normal" multiline signal (data not shown). The absence of a light-induced multiline signal after illumination at 200 K is in accord with the reported characteristics of these preparations (Ono & Inoue, 1989) and is also evidence of the completeness of inhibition and the lack of contaminating Ca at a concentration high enough to reactivate a detectable number of the Mn centers to a Ca-sufficient/"normal" multiline state.

Mn K-Edge Spectroscopy. Mn X-ray K-edge spectra for Ca- and Sr-reactivated samples in the S_1 state are presented in Figure 2. The two edges are almost superimposable, and the edge inflection energies, taken from the second-derivative zero crossing, are within 0.2 eV of each other, with the edge in Sr-PS II slightly higher than that in Ca-PS II. The second-derivative spectra show that the overall edge shapes are also

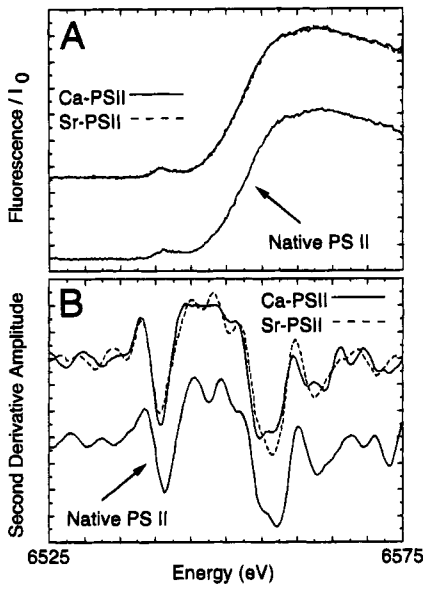

FIGURE 2: Mn K-edge X-ray absorption spectra of Ca- (solid line) and Sr-reactivated (dashed line) PS II in the S_1 state. Absorption spectra are presented in (A) and second derivatives in (B). The edges from Ca- and Sr-reactivated samples are virtually identical to each other and also to untreated PS II samples. The shapes of the edges are accentuated in the second-derivative spectra (B) where, again, all three types of samples are shown to give similar spectra.

quite similar (Figure 2B); furthermore, no differences in shape or edge inflection energy are found between these samples and control samples of untreated PS II in the S_1 state (also displayed in Figure 2). The similarity of the edges provides evidence that there has been no significant change in the oxidation state or ligand environment/symmetry of the Mn cluster in Ca-PS II and Sr-PS II relative to untreated preparations. The observation that the edges are similar is also significant in that the modifications to the multiline signal and the lower rates of oxygen evolution in Sr-reactivated preparations do not appear to arise from a very different environment or oxidation level for the Mn ions in PS II.

Mn EXAFS of Ca- and Sr-Reactivated Preparations in the S_1 State. Background-subtracted EXAFS oscillations in k-space for Ca-PS II and Sr-PS II (data multiplied by k^3) are presented in Figure 3. Both data sets are of comparable signal-to-noise ratios and are similar except for small differences in EXAFS position and amplitude at about 9.3 and 11 Å^{-1}. The data are multiplied by k^3, which offsets the decay of EXAFS amplitudes at higher values of k and also emphasizes the contributions of scattering atoms at longer distance and of higher atomic number (Teo, 1986).

All data sets were truncated to $k = 11.2$ Å^{-1} to exclude a glitch that appeared as a spike in the data at about 11.3 Å^{-1}. Glitches are caused by a sudden drop in X-ray intensity and are a property of the particular crystal set (Si⟨220⟩) used in the double-crystal monochromator.

The Fourier transforms of the k-space data are presented in Figure 4. Three peaks appear at $R' = 1.3$, 2.3, and 3.0 Å that are above the noise level, and there is possibly a fourth peak at about 3.8 Å. The peaks appear at an apparent distance (R') that is shorter than the actual distances in the complex due to a phase shift caused by the effect of the potentials of the absorbing and scattering atoms on the photoelectron. Actual distances are determined through

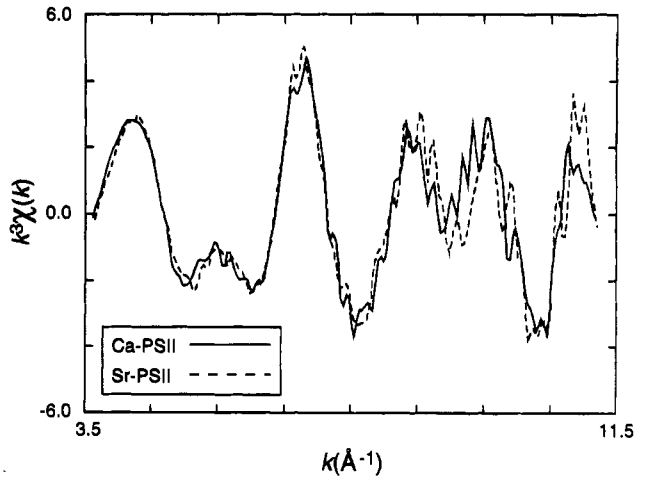

FIGURE 3: Background-subtracted k-space EXAFS data from Ca- and Sr-reactivated PS II. These data have been multiplied by k^3. Differences in the EXAFS between Ca- and Sr-reactivated samples are clear at $k = 9.3$ and 11 Å^{-1}.

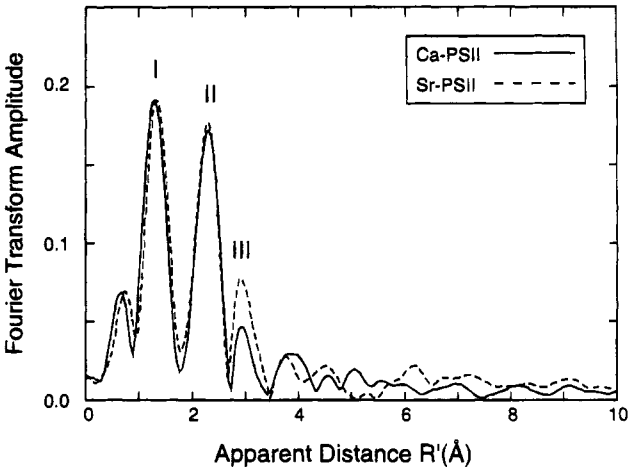

FIGURE 4: Fourier transform power spectra of k-space data presented in Figure 3. The major Fourier peaks are labeled I, II, and III. The spectra are clearly different in the amplitude of peak III, which is enhanced in the spectrum from the Sr-reactivated sample.

curve fitting of the EXAFS oscillations. The good signal-to-noise ratio of the data is reflected by the absence of major peaks from the Fourier transform in the $R' = 5-10$ Å region. The small peak at an apparent distance of 0.8 Å is a result of incomplete background removal.

The three peaks and the apparent distances at which they appear are similar to those reported for low-temperature Mn EXAFS from a variety of PS II preparations (Penner-Hahn et al., 1990; George et al., 1989; Sauer et al., 1992; Yachandra et al., 1993; Mukerji et al., 1994; DeRose et al., 1994). It is generally agreed that the first peak corresponds to oxygen or nitrogen scatterers at about $R = 1.8-2.1$ Å, the second peak is due to Mn at about 2.7 Å, and the third peak is due to scatterers at distances >3 Å. The most obvious difference in these data is a change in the amplitude of peak III in the Sr-reactivated sample vs the Ca-reactivated sample.

We have used several different background removal techniques (splines in energy or k-space) and different ranges of k-space data for transformation, and we find the same pattern of peaks in the Fourier transform, including the change in amplitude of peak III between Ca-PS II and Sr-

Table 1: Two-Shell Simulations of Fourier Peaks I and II[a]

	Mn−O interaction			Mn−Mn interaction					
sample[b]	$R(1)$ (Å)	$N(1)$	$\sigma^2(1)$[c]	$R(2)$ (Å)	$N(2)$	$\sigma^2(2)$	ΔE_0	Φ ($\times 10^3$)[d]	ϵ^2 ($\times 10^5$)[d]
Ca1	1.83	2.62	0.0051	2.70	1.04	0.0020	−22	0.53	4.22
Ca2	1.83	1.90	0.0037	2.70	0.95	0.0020	−22	0.53	4.16
Sr1	1.83	2.55	0.0056	2.70	0.93	0.0016	−23	0.29	2.28
Sr2	1.83	2.10	0.0036	2.69	0.88	0.0020	−24	0.27	2.14
Sr3	1.85	2.66	0.0051	2.70	0.94	0.0012	−21	0.28	2.23

[a] Fit parameters are as defined in the text. $S_0^2 = 0.85$ in all fits. Data were fit from $k = 4.5$ to 10.5 Å^{-1}. The width of the Fourier isolation window employed was 2 Å. [b] Ca1 and Ca2 are Ca-reactivated samples; Sr1, Sr2, and Sr3 are Sr-reactivated samples. [c] Units are square angstroms. [d] Goodness of fit parameters Φ and ϵ^2 are defined in Materials and Methods.

Table 2: One-Shell (Mn−Mn) Simulations of Fourier Peak II[a]

sample[b]	R (Å)	N	σ^2 (Å^2)[c]	ΔE_0	Φ ($\times 10^3$)[d]	ϵ^2 ($\times 10^5$)[d]
Ca1	2.74	1.00	0.002	−15	0.23	0.71
Ca2	2.74	0.93	0.002	−14	0.13	0.39
Sr1	2.72	1.00	0.002	−17	0.19	0.59
Sr2	2.72	0.84	0.002	−18	0.17	0.53
Sr3	2.72	0.95	0.002	−18	0.20	0.61

[a] Fit parameters are as defined in the text. $S_0^2 = 0.85$ in all fits. Data were fit from $k = 4.5$ to 10.5 Å^{-1}. The width of the Fourier isolation window employed was 1.0 Å. [b] Samples as defined in Table 1. [c] Parameter is fixed in the fit. [d] Goodness of fit parameters Φ and ϵ^2 are defined in Materials and Methods.

PS II. Thus, this effect is unlikely to arise from truncation artifacts or background removal procedures and corresponds to real differences between the data sets.

The change in the amplitude of peak III has been observed in three other data sets that we have acquired on the same type of samples (data not shown). Of five Sr-reactivated samples, only one has shown no significant increase in the third-peak amplitude. One of the four that displayed an increase in peak III was not used for curve fitting due to the presence of crystal glitches, which were difficult to remove from the spectrum.

Curve Fitting of Mn EXAFS Data. Curve-fitting results for the EXAFS data from five samples, two Ca-reactivated (Ca1, Ca2) and three Sr-reactivated (Sr1, Sr2, Sr3) samples, are presented in Tables 1−5.

Peaks I and II. The first and second Fourier peaks were isolated together and fit as a combination of two or three shells of scatterers. The results of the curve-fitting procedure for these two peaks are presented in Table 1. Overall the results are similar to those presented previously (Sauer et al., 1992; Penner-Hahn et al., 1990; George et al., 1989; MacLachlan et al., 1992; Yachandra et al., 1993; DeRose et al., 1994). Two shells of scatterers were needed to fit the data: a shell of about two O or N atoms at 1.83−1.85 Å and a shell of about 1.0 Mn at about 2.7 Å. Unlike our previous work with native samples (Sauer et al., 1992; Yachandra et al., 1993; DeRose et al., 1994), addition of a disordered third shell of O or N at 1.9−2.1 Å does not significantly improve the simulation for these reconstituted samples. The first peak thus appears to be dominated by an O or N 1.83−1.85 Å interaction.

Fitting parameters for Fourier peak II alone are presented in Table 2 and agree well with our earlier results on untreated PS II, where the peak was fit as a shell of ~1.2 Mn at ~2.7 Å (Sauer et al., 1992; Yachandra et al., 1993; DeRose et al., 1994). There is a small, consistent difference in the distance of the Mn−Mn ~2.7 Å interaction between Ca- and Sr-PS II. Ca-reactivated samples fit to a slightly longer distance (0.01−0.02 Å longer) than Sr-reactivated samples. This slightly longer distance in Ca-reactivated samples was found in fits to isolates of peak II, peaks I and II together, and peaks II and III together, although the exact distance determined in each fit differs somewhat depending upon the type of fit (peaks I and II, peak II alone, or peaks II and III). This difference, although within the experimental error for each individual fit, is observed consistently and probably corresponds to a real difference in the data.

Peak III. The major difference observed in the EXAFS from Ca- and Sr-reactivated samples is the apparent difference in amplitude of peak III in the Fourier transforms (see Figure 4). In fitting peak III, we have tried to evaluate possible models for the Mn cluster, depending not only on the mathematical quality of the fit but also on the ability of the models and fit parameters to provide a chemically reasonable physical description of the observed differences between Ca- and Sr-reactivated samples. Fits to peak III are difficult because the third shell contributes a relatively small portion of the total EXAFS and arises from scatterers at a distance (about 3.2−3.5 Å) where there are many possible contributions from low-Z atoms. Glutamate and aspartate residues, which are likely components of the ligand environment for the Mn cluster in PS II, have a number of C and O atoms either two or three bonds away from the liganding atom, which would fall in the range 3−3.5 Å. Multiple contributions to a single Fourier peak complicate the fitting and result in greater uncertainties in the fit parameters (Scott & Eidsness, 1988). The quality of fits to the third shell is also proportionately more susceptible to the noise level in the data.

It should also be noted that Fourier isolation of such a small feature as peak III can cause distortions due to the limited range of data used in the isolation (about 0.8 Å) and to the presence of a much larger neighboring peak (the Mn−Mn 2.7 Å interaction). Isolation of a larger range of data can help to reduce distortions, but use of a range including the larger Mn−Mn 2.7 Å interaction results in simulations that are less sensitive to the composition of peak III. The fits presented here are of Fourier isolates of peaks II and III together, although we have performed fits on peak III alone with similar results.

In Table 3 we consider the simplest models for the identity of scatterers comprising peak III: models where a single type of scatterer is present. For each type of fit, Debye−Waller factors (σ^2) were fixed to reasonable values, thus allowing comparisons of coordination numbers between samples. The parameters describing peak II (considered to be a Mn−Mn ~2.7 Å interaction) in each fit are relatively constant for each type of scatterer considered for peak III. In each case, the peak II fit values indicate a slightly shorter distance in Sr-reactivated samples (by 0.01−0.02 Å), which is consistent with the results observed in fits to peak II alone, although the absolute distances fit differ somewhat depending on the scatterer chosen for peak III.

The best single-shell fits to peak III for Ca-reactivated samples are obtained by using a Mn shell at about 3.31 Å (Table 3, fits A), although equivalent fits to the data can also be obtained with a Ca shell at ~3.37 Å (Table 3, fits B). Samples containing Sr, however, show somewhat better

Table 3: Two-Shell Simulations of Fourier Peaks II and III[a]

	Mn−Mn interaction			Mn−Mn interaction					
sample[b]	$R(1)$ (Å)	$N(1)$	$\sigma^2(1)$[c]	$R(2)$ (Å)	$N(2)$	$\sigma^2(2)$[c]	ΔE_0	Φ ($\times 10^3$)[d]	ϵ^2 ($\times 10^5$)[d]
Fits A									
Ca1	2.75	1.18	0.003	3.31	0.48	0.004	−12	0.18	0.44
Ca2	2.76	1.09	0.003	3.32	0.58	0.004	−11	0.13	0.31
Sr1	2.74	1.18	0.003	3.31	0.89	0.004	−11	0.27	0.66
Sr2	2.74	0.99	0.003	3.30	0.76	0.004	−13	0.30	0.72
Sr3	2.74	1.06	0.003	3.29	0.73	0.004	−14	0.33	0.80
	Mn−Mn interaction			Mn−Ca interaction					
sample[b]	$R(1)$ (Å)	$N(1)$	$\sigma^2(1)$[c]	$R(2)$ (Å)	$N(2)$	$\sigma^2(2)$[c]	ΔE_0	Φ ($\times 10^3$)[d]	ϵ^2 ($\times 10^5$)[d]
Fits B									
Ca1	2.75	1.16	0.003	3.37	0.60	0.004	−12	0.18	0.44
Ca2	2.75	1.07	0.003	3.38	0.72	0.004	−11	0.13	0.32
Sr1	2.74	1.15	0.003	3.37	1.09	0.004	−11	0.31	0.75
Sr2	2.74	0.95	0.003	3.35	0.93	0.004	−13	0.33	0.80
Sr3	2.73	1.08	0.003	3.34	0.90	0.004	−14	0.36	0.87
	Mn−Mn interaction			Mn−Sr interaction					
sample[b]	$R(1)$ (Å)	$N(1)$	$\sigma^2(1)$[c]	$R(2)$ (Å)	$N(2)$	$\sigma^2(2)$[c]	ΔE_0	Φ ($\times 10^3$)[d]	ϵ^2 ($\times 10^5$)[d]
Fits C									
Sr1	2.71	1.10	0.003	3.51	0.74	0.004	−18	0.22	0.54
Sr2	2.71	0.91	0.003	3.49	0.60	0.004	−19	0.29	0.70
Sr3	2.71	1.04	0.003	3.48	0.60	0.004	−20	0.28	0.67
	Mn−Mn interaction			Mn−C interaction					
sample[b]	$R(1)$ (Å)	$N(1)$	$\sigma^2(1)$[c]	$R(2)$ (Å)	$N(2)$	$\sigma^2(2)$[c]	ΔE_0	Φ ($\times 10^3$)[d]	ϵ^2 ($\times 10^5$)[d]
Fits D									
Ca1	2.75	1.01	0.002	3.32	2.13	0.002	−11	0.20	0.48
Ca2	2.76	0.94	0.002	3.33	2.63	0.002	−10	0.14	0.34
Sr1	2.75	1.01	0.002	3.33	3.91	0.002	−10	0.30	0.73
Sr2	2.74	0.84	0.002	3.31	3.37	0.002	−12	0.33	0.80
Sr3	2.73	0.96	0.002	3.29	3.29	0.002	−13	0.33	0.80

[a] Fit parameters are as defined in the text. $S_0^2 = 0.85$ in all fits. Data were fit from $k = 4.5$ to 10.5 Å^{-1}. The width of the Fourier isolation window employed was 1.8 Å. [b] Samples as defined in Table 1. [c] Parameter is fixed in the fit. Units are square angstroms. [d] Goodness of fit parameters Φ and ϵ^2 are defined in Materials and Methods.

fit quality for a single shell of Sr (Table 3, fits C) than for fits to Ca or Mn (Φ values, Table 3). Finally, all samples were fit to C at about ~3.32 Å; both a well-ordered shell (Table 3, fits D) and a disordered shell were considered. Within this model, the well-ordered C shell ($\sigma^2 = 0.002$) fit much better than the disordered C shell ($\sigma^2 = 0.010$, data not shown). If Debye−Waller factors were allowed to vary for the C shell, all the σ^2 values went to 0.

Previously, peak III was proposed to be due primarily to a Mn at 3.3 Å (George et al., 1989; DeRose et al., 1994), a Mn or Ca at 3.3 Å (Penner-Hahn et al., 1990), a Ca at about 3.7 Å (MacLachlan et al., 1992), or a Mn and a Ca at about 3.3 Å (Yachandra et al., 1993; DeRose et al., 1994). A Mn−Mn interaction was thought by most authors to be the most likely component, due to both slightly better fits to the EXAFS of native samples and the fact that similar Mn−Mn distances have been observed in synthetic manganese complexes (Wieghardt et al., 1985; Sheats et al., 1987) where the Mn atoms are bridged by a mono-μ-oxo bridge and one or more bidentate carboxylate ligands.

The fits presented in Table 3 must be evaluated by taking into account all of the information known about the samples and also by keeping in mind chemically reasonable structural models. Although satisfactory fits to the peaks II and III isolate can be obtained with two shells (Mn−Mn at ~2.7 Å and Mn−Mn/Ca/Sr at 3.3−3.5 Å), it is difficult to explain the differences observed in the amplitude of peak III in Ca- vs Sr-reactivated samples in a chemically reasonable way. For example, the fits to a single shell of Mn imply that reactivation with Sr results in an increase in the Mn−Mn coordination number from ~0.5 in Ca-reactivated samples to ~0.8 in Sr-reactivated samples (Table 3, fits A). One could propose that some of the Mn clusters have lost the Mn−Mn ~3.3 Å interactions in the Ca-reactivated sample relative to the Sr-reactivated sample, but Ca reactivates samples more completely (higher O_2 evolution rates, restoration of "native" multiline EPR signal) than does Sr. It is unlikely that a structural feature of the native complex would be diminished in a Ca-reactivated sample, which is closer in activity and chemical composition to a native sample, relative to a Sr-reactivated sample.

Coordination numbers and Debye−Waller factors within a shell are strongly correlated in EXAFS curve fitting, and we find that it is also possible to fit both Ca- and Sr-reactivated samples using the same Mn coordination number for the ~3.3 Å Mn−Mn interaction. In this case, the difference between data sets is reflected in an increased Debye−Waller factor in Ca-reactivated samples relative to Sr-reactivated samples, although the fit quality is as good (data not shown). Debye−Waller parameters describe both static and thermal disorder, and because the measurements were taken at low temperature and the basic structure appears to remain intact, increased disorder would have to be the result of an increase in the static term. There is no reason, however, to suppose that a single Mn−Mn interaction in the Mn cluster in Ca-reactivated PS II would be any more disordered than in Sr-reactivated PS II because, if anything, Ca binds better than Sr and therefore should result in a more homogeneous Mn cluster. Thus, although increased static disorder is a possible explanation of the differences in the data sets, it is difficult to reconcile with a physical model.

We have observed decreases in amplitude of peak III in spectra from native samples exhibiting the $g = 4$ S_2-state EPR signal (Liang et al., 1994) and ammonia-treated samples in the S_2 state (Dau et al., 1995). In both cases, the decreases could be ascribed to increased distance heterogeneity in peak III, indicating that a single Mn−Mn interaction is unlikely. A more reasonable scenario to consider, as did Liang et al. (1994), is more than one Mn−Mn interaction at ~3.3 Å (see the following).

The same situation of increased coordination number for Sr- vs Ca-reactivated samples also occurs for fits to Ca and C. In the case of a Mn−Ca interaction (Table 3B), an increased coordination number for Ca in the Sr-reactivated sample ($N = 0.9-1.09$ vs 0.6−0.72 in the Ca-reactivated sample) is a virtual impossibility because the sample had been specifically depleted of Ca and reactivated with a relatively high concentration of high-purity $SrCl_2$. Again, increased disorder can also be considered, but the fit quality is worse and this seems unlikely for the some of the same reasons given for a Mn−Mn interaction. In the case of a C shell, a disordered shell provides a very poor fit to the data (fit parameters not shown). A well-ordered C shell (Table 3D), while not fitting the data as well Mn or Ca, also results in an increased coordination number for Sr- ($N = 3.3-3.9$) vs Ca-reactivated samples ($N = 2.1-2.6$). Again, there is

no satisfactory model to account for the change, and, in addition, the results are suggestive that there would need to be 2−4 C atoms/Mn in a well-defined shell at ~3.4 Å. That would be a total of 8−16 Mn−C interactions with a very small distance spread, which is an extremely unlikely situation in a protein where the coordination environment beyond the first ligand sphere would be expected to be relatively disordered. A distributed spread of C/N/O interactions resulting in a disordered shell(s) that could be smeared out beyond the detectable limits of EXAFS would be more likely.

The Sr-reactivated samples were also fit to a shell of Sr to test the possibility that the change in amplitude of peak III was the result of an exchange of Sr for Ca (Table 3, fits C). The fit quality to a single shell of Sr for Sr-reactivated samples is better than that of fits to Ca or Mn by 10−30% (see Φ values, Table 3). The best fits were found at a distance of ~3.5 Å with a coordination number comparable to that found in Ca-reactivated samples fit with a Ca shell ($N = 0.6-0.74$). This would correspond to ~2−3 Mn−Ca or −Sr interactions in the Mn complex and is consistent with a model wherein Ca is replaced by Sr. The increased fit distance (~3.5 Å for Sr vs ~3.4 Å for Ca) makes sense in that the ionic radius of Sr is 0.1 Å larger than that of Ca. The relatively large coordination number for Ca/Sr (2−3 Mn−Ca/Sr interactions) implies that there is either a single Ca/Sr site with multiple Mn−Ca/Sr interactions, all at about the same distance, or several sites with the same Mn−Ca/Sr distances. The low-pH treatment that we employed to deplete Ca from PS II has been reported to remove only one of the two Ca ions in PS II (Ono & Inoue, 1988); thus, a single site is a more reasonable interpretation. In either case, several Mn−Ca/Sr vectors of the same distance would need to be present, which is an unlikely, though still possible, model.

Because it is difficult to rationalize the results of the previous fits, we undertook more complicated three-shell fits to the data considering two models: one where both Mn−Mn and Mn−Ca/Sr interactions are present in peak III (Mn + Ca/Sr model) and one where two Mn−Mn interactions (2 Mn model) are present. The small data range available for fitting limits the number of free parameters allowed in a given fit (see Materials and Methods) and precludes adding shells with more free parameters. To address this problem, in the following fits we have fixed coordination numbers and σ^2 values to allow fitting to specific, chemically reasonable models. The only free parameters were distances and a single ΔE_0 for each fit.

It should be noted that, although the more complicated models include another scattering shell employing a larger total number of parameters than the fits presented in Table 3, the actual number of freely floating parameters is smaller (4 vs 5). The different numbers of fixed and floating parameters complicate direct comparisons of fit quality between two- and three-shell simulations. Differences in fit quality parameters (Φ and ϵ^2) between two- and three-shell fits are noted to show whether a given simulation follows the data as well as another, but they do not necessarily provide proof that one model is superior. However, differences in fit quality between fits with the same number of shells can be more directly interpreted.

The results of fits for the Mn + Ca/Sr model are presented in Table 4. All data sets were fit to shells of Mn at ~2.7 and 3.3 Å and a shell of Ca at 3.3−3.5 Å (Table 4, fits A). The quality of fits to the Ca-reactivated samples is equal to or better than that of all of the fits in Table 3 (see Φ values, Table 3, for fits to Ca1 and Ca2 samples). Greater improvement is seen in the ϵ^2 values for Table 4 vs Table 3 fits, the reason being that, although there were more shells being fit, there was actually one less free parameter in the fits in Table 4 than in those in Table 3. The Sr-reactivated samples, when fit to Mn and Ca shells (Table 4, fits A), fit to a shorter Ca distance (~3.34 Å) than the Ca-reactivated samples (~3.46 Å); the EXAFS changes between Ca- and Sr-reactivated PS II are reflected in the decreased difference in distance (lessened disorder) between the Ca and Mn shells in the Sr-reactivated samples. Sr-reactivated samples were also fit with a Sr shell instead of a Ca shell (Table 4, fits B). For all of the Sr-reactivated samples, the fit quality was improved (20−25% decrease in Φ) by changing the Ca shell to a Sr shell (Table 4). The fit quality for two out of three of the Sr samples was better than the best fits in Table 3 (fits C), decreasing Φ by ~20%. As in the case with the single-shell Ca/Sr fits (Table 3B,C), the Sr distance is longer (3.54 Å) than the Ca distance (3.46 Å), which fits well with a model where Sr (with a larger ionic radius) has been substituted for Ca in a binding site closely associated with the Mn cluster. Fits based on the Mn + Ca/Sr model are displayed in Figure 5A (Ca-reactivated sample) and 5B (Sr-reactivated sample). The differences in the EXAFS of the two samples, most apparent in the beat pattern at $k = 8$ Å^{-1}, are well-simulated by the change of one Mn−Ca interaction for a Mn−Sr interaction. The individual EXAFS waves for the Ca contribution in Figure 5A and the Sr contribution in Figure 5B are overplotted in Figure 5C and clearly show that the waves are different in both phase and amplitude.

The fits to the 2 Mn model are presented in Table 5. In this case we consider the possibility that there is more than one Mn−Mn interaction giving rise to peak III. To test this possibility, the data were fit using a single Mn shell for peak III with a larger coordination number, fixed at 1.0, corre-

Table 4: Three-Shell Simulations of Fourier Peaks II and III, Mn and Ca Model[a]

	Mn−Mn		Mn−Mn		Mn−Ca				
sample[b]	$R(1)$ (Å)	$N(1)$[c]	$R(2)$ (Å)	$N(2)$[c]	$R(3)$ (Å)	$N(3)$[c]	ΔE_0	Φ (×10³)[d]	ϵ^2 (×10⁵)[d]
Fits A									
Ca1	2.75	1.0	3.29	0.5	3.47	0.25	−11	0.18	0.29
Ca2	2.75	1.0	3.30	0.5	3.46	0.25	−11	0.12	0.19
Sr1	2.74	1.0	3.31	0.5	3.36	0.25	−11	0.24	0.38
Sr2	2.74	1.0	3.28	0.5	3.36	0.25	−14	0.43	0.69
Sr3	2.73	1.0	3.29	0.5	3.30	0.25	−14	0.26	0.42
	Mn−Mn		Mn−Mn		Mn−Sr				
sample[b]	$R(1)$ (Å)	$N(1)$[c]	$R(2)$ (Å)	$N(2)$[c]	$R(3)$ (Å)	$N(3)$[c]	ΔE_0	Φ (×10³)[d]	ϵ^2 (×10⁵)[d]
Fits B									
Sr1	2.73	1.0	3.28	0.5	3.55	0.25	−14	0.18	0.28
Sr2	2.72	1.0	3.25	0.5	3.54	0.25	−17	0.36	0.58
Sr3	2.72	1.0	3.24	0.5	3.53	0.25	−17	0.21	0.33

[a] Fit parameters are as defined in the text. $S_0^2 = 0.85$ in all fits. Data were fit from $k = 4.5$ to 10.5 Å^{-1}. The width of the Fourier isolation window employed was 1.8 Å. For all fits $\sigma^2(1) = 0.002$ Å^2 and $\sigma^2(2) = \sigma^2(3) = 0.003$ Å^2. [b] Samples are as defined in Table 1. [c] Coordination numbers were fixed in the fit. [d] Goodness of fit parameters Φ and ϵ^2 are defined in Materials and Methods.

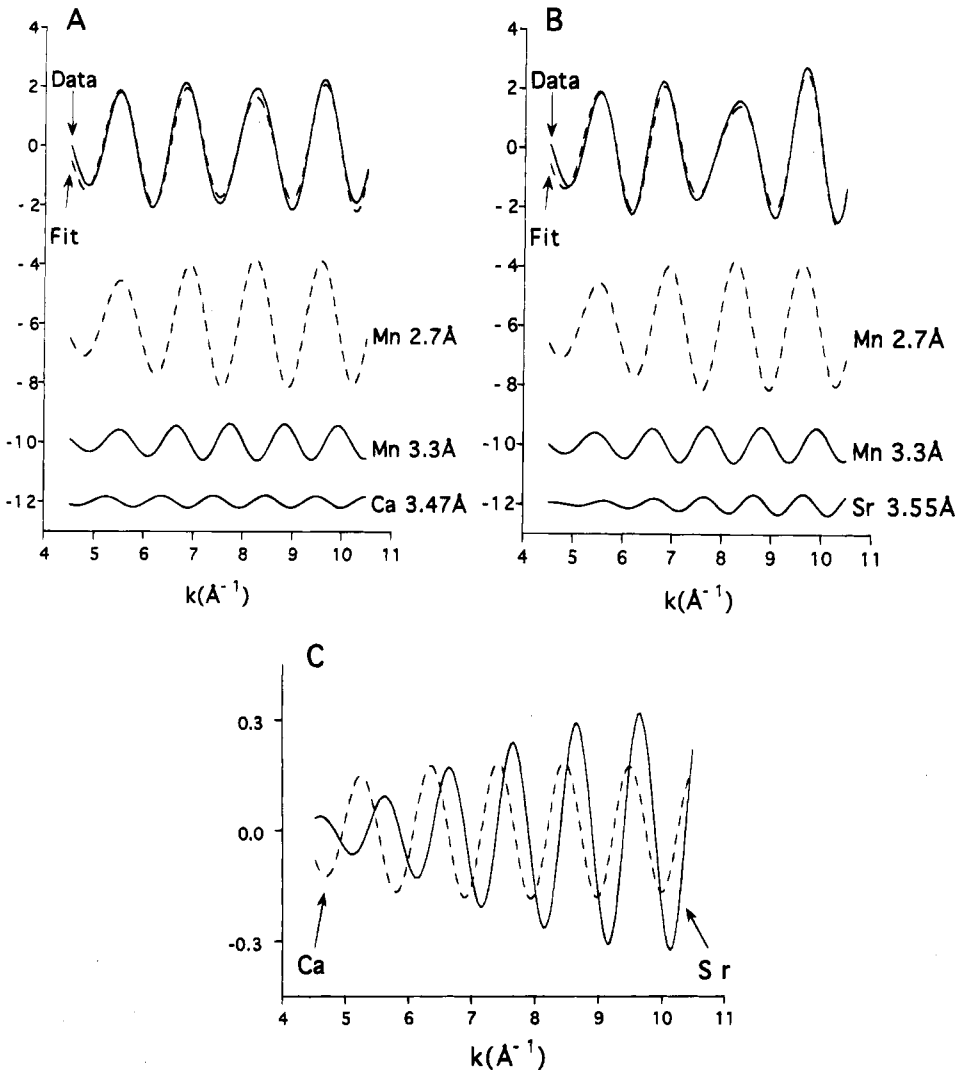

FIGURE 5: Fits to the EXAFS of Ca- and Sr-reactivated PS II. Both fits are to Fourier isolates of peaks II and III. The parameters used for the fit are found in Table 4. The fit to the Ca-reactivated sample (A) was calculated by using the fit values for the Ca1 sample in Table 4A. The fit to the Sr-reactivated sample was calculated by using fit values for the Sr1 sample in Table 4B. The partial waves due to individual scattering contributions are shown as well as the overall fit (top). The individual Ca and Sr partial waves used in these fits are overplotted (C) and demonstrate clear differences in phase and amplitude for these two contributions.

sponding to two Mn−Mn interactions (Table 5, fits A). In these fits, the Debye−Waller parameter for the ~3.3 Å Mn shell was allowed to float and indicated larger disorder for the Ca-reactivated samples relative to the Sr-reactivated samples by a factor of almost 2. In the fits labeled B (Table 5), the Mn shell at ~3.3 Å was split into two equal Mn−Mn interactions, representing the same total number of Mn−Mn interactions at ~3.3 Å as in the A fits. The spread of Mn−Mn distances in fits to peak III is slightly greater in the Ca-reactivated samples (0.14 Å) than in the Sr-reactivated samples (0.09 Å), possibly accounting for the difference in amplitude of peak III in the Fourier transforms. Although these fits do describe another reasonable structural model to explain the differences between the Ca- and Sr-reactivated data sets, the fit quality is no better for two Mn shells (Table 5B) than for one disordered Mn shell (Table 5A). This is in contrast to the Mn + Ca/Sr model in which the fit quality was improved by the change of a Ca shell for a Sr shell in the Sr-reactivated samples. In addition, the fit quality for the Sr-reactivated samples is worse (by 30−40%) for the 2 Mn fits (Table 5B) than for the Mn + Ca/Sr fits (Table 4B). The 2 Mn fits and the Mn + Ca/Sr fits are directly comparable in terms of their numbers of fixed and floating fit parameters.

DISCUSSION

The results presented earlier indicate that the dominant effect of reactivation of calcium-depleted preparations with strontium rather than calcium is a change in the environment of the manganese cluster at a distance greater than 3 Å. We suggest that the data presented here are best explained by the replacement of Ca by Sr in a binding site in close proximity to the Mn cluster in PS II for the following reasons.

(1) The Mn K-edge spectra indicate that no major changes have occurred in the oxidation states or ligand environments of the manganese ions in Ca- or Sr-reactivated PS II relative to those in untreated preparations. The similarity of the first two peaks in the EXAFS from calcium- and strontium-reactivated preparations to those in untreated preparations is also an indication that the manganese cluster has been restored to an intact state. The fact that high rates of oxygen evolution in these preparations are restored to the same extent, albeit with altered kinetics, for Sr-reactivated prepara-

Table 5: Three-Shell Simulations of Fourier Peaks II and III, 2 Mn 3.3 Å Model[a]

	Mn−Mn		Mn−Mn					
sample[b]	$R(1)$ (Å)	$N(1)$[c]	$R(2)$ (Å)	$N(2)$[c]	$\sigma^2(2)$ (Å^2)	ΔE_0	Φ ($\times 10^3$)[d]	ϵ^2 ($\times 10^5$)[d]
Fits A								
Ca1	2.74	1.0	3.29	1.0	0.0103	−12	0.16	0.25
Ca2	2.75	1.0	3.32	1.0	0.0081	−11	0.13	0.20
Sr1	2.74	1.0	3.31	1.0	0.0048	−10	0.24	0.38
Sr2	2.74	1.0	3.28	1.0	0.0054	−14	0.46	0.72
Sr3	2.73	1.0	3.28	1.0	0.0058	−14	0.30	0.47

	Mn−Mn		Mn−Mn		Mn−Mn				
sample[b]	$R(1)$ (Å)	$N(1)$[c]	$R(2)$ (Å)	$N(2)$[c]	$R(3)$ (Å)	$N(3)$[c]	ΔE_0	Φ ($\times 10^3$)[d]	ϵ^2 ($\times 10^5$)[d]
Fits B									
Ca1	2.74	1.0	3.37	0.5	3.22	0.5	−12	0.15	0.24
Ca2	2.75	1.0	3.38	0.5	3.26	0.5	−11	0.12	0.19
Sr1	2.74	1.0	3.36	0.5	3.28	0.5	−10	0.24	0.38
Sr2	2.74	1.0	3.33	0.5	3.24	0.5	−14	0.46	0.72
Sr3	2.73	1.0	3.33	0.5	3.23	0.5	−14	0.30	0.47

[a] Fit parameters are as defined in the text. $S_0^2 = 0.85$ in all fits. Data were fit from $k = 4.5$ to 10.5 Å^{-1}. The width of the Fourier isolation window employed was 1.8 Å. For A fits $\sigma^2(1) = 0.002$ Å^2; for B fits $\sigma^2(1) = 0.002$ Å^2 and $\sigma^2(2) = \sigma^2(3) = 0.003$ Å^2. [b] Sample identification as in Table 1. [c] Coordination numbers were fixed in the fits. [d] Goodness of fit parameters Φ and ϵ^2 are defined in Materials and Methods.

tions is a further indication that substitution of Sr for Ca results in no major changes in the structure of the complex.

(2) EPR spectra of Sr-reactivated samples show an altered multiline signal and an enhanced $g = 4$ signal relative to Ca-reactivated samples. These changes clearly indicate an effect directly on the Mn cluster caused by the substitution of Ca by Sr. The Sr-altered multiline is similar to the multiline observed in ammonia-inhibited PS II, where ammonia has been shown to bind directly to manganese (Britt et al., 1989). It has been proposed that the modifications in the EPR spectra are caused by the replacement of Ca by Sr in a binding site close to the Mn complex (Boussac & Rutherford, 1988a,b).

(3) Finally, the differences in the EXAFS spectra between the Ca-PS II and Sr-PS II data sets can be ascribed to the change of Ca to Sr approximately 3.4 Å from a manganese ion. This a reasonable proposition given the chemical differences between the two preparations (just the presence of Ca or Sr). The enhanced X-ray photoelectron backscattering cross section of Sr vs Ca is a plausible explanation for the amplitude change in the third Fourier peak in the EXAFS. The data can be fit with Ca/Sr as the sole contributor to Fourier peak III or with Mn + Ca/Sr contributing to peak III. From the structural analyses we present here, we view the most likely model to be one in which both Mn−Ca and Mn−Mn interactions contribute to peak III.

The differences in the EXAFS between the Ca-reactivated and Sr-reactivated data sets can also be simulated as a change in the number of Mn scatterers contributing to the third peak, but this is difficult to reconcile in a chemically reasonable physical model. More Mn−Mn interactions would probably require a relatively major change in the structure of the complex, possibly resulting in more oxo bridges. The difference in coordination number also is not sufficient to account for a stoichiometric increase in Mn−Mn interactions.

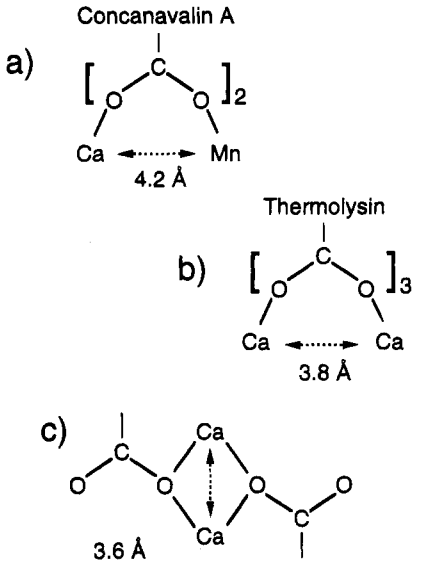

FIGURE 6: Ca−metal-bridging structures and distances for several structurally characterized systems: (a) concanavalin A (Edelman et al., 1972; Hardman & Ainsworth, 1972); (b) thermolysin (Matthews et al., 1974); (c) garcinia acid (Glusker et al., 1971).

An alternative explanation is that the difference between data sets arises from a lack of reactivation of centers in Ca-PS II relative to Sr-PS II, leading to decreased Mn−Mn coordination numbers in Ca-PS II, but this is also difficult to reconcile with the facts that reactivation of O_2 evolution is greater in Ca-PS II than in Sr-PS II and that Ca reactivates with higher binding affinity and produces a "native"-like multiline EPR signal.

We also consider a model where two Mn−Mn interactions at slightly different distances contribute to peak III. This is another reasonable structural model, but there was no improvement in the fit quality for two Mn−Mn shells vs fits to a single disordered Mn−Mn shell, and the data were not fit as well as they were by the Mn + Ca/Sr model.

The preceding interpretations require a note of caution. Even the most complicated models presented here (peak III comprising two metal−metal interactions) are simplifications in that they do not include C/N/O contributions, which, although almost certainly disordered, must be present in the complex. In fitting these data we are also rather severely information-limited due to the small k-range of the data and the relatively small contribution that peak III makes to the total EXAFS. More complicated models including more metal−metal interactions or large numbers of individual C/N/O shells, although certainly possible, cannot be critically evaluated on the basis of the data presented here. The Mn + Ca/Sr model for peak III does, however, describe our data well and provides a chemically reasonable explanation for the differences observed in the EXAFS of Ca- and Sr-reactivated samples.

The manganese−calcium distance that we propose from the EXAFS results presented here is rather short for a calcium−metal interaction. A calcium-binding site at this distance from another metal ion (~3.4 Å) has, to our knowledge, not been reported in other biological systems, but an examination of protein calcium-binding sites and calcium complexes of known structure provides clues as to the structural possibilities that might give rise to such an interaction (the following structures are summarized in Figure 6).

The manganese–calcium-binding site of concanavalin A, in which two carboxyl groups bridge between Mn and Ca, has a metal–metal distance of 4.2 Å (Edelman et al., 1972; Hardman & Ainsworth, 1972). A close association between two calcium ions is found in thermolysin, which has a binding site in which two calcium ions are bridged by three carboxyl groups, resulting in a metal–metal distance of 3.8 Å (Matthews et al., 1974). Closer associations have been observed in calcium complexes when two metal atoms share the same oxygen atom. In the calcium salt of garcinia acid, a Ca–Ca distance of 3.6 Å can be found where the two Ca are bridged by single oxygen atoms from two carboxyls (Glusker et al., 1971). Finally, we note that Bonadies et al. (1989) have reported a manganese complex containing sodium in which the Mn–Na distance is 3.3 Å. The Mn and Na ions are bridged by one acetate molecule and two oxygen atoms from phenolate groups. Although Mn is bridged to Na and not to Ca, this structure has relevance because Na has an ionic radius equal to that of Ca. The Ca–Ca structures pictured would probably have shorter metal–metal distances if one of the metals was a high-valent Mn ion (i.e., Mn^{3+} or Mn^{4+}), which can exhibit a range of Mn-bridging O distances from 1.75 to 1.9 Å (Pecoraro, 1992; Wieghardt, 1989).

Given the preceding structures, it seems probable that a calcium–metal interaction at 3.4–3.5 Å would involve one or more bridging atoms, probably oxygen. Bridging oxygen atoms could be derived from the carboxyl groups of aspartate, glutamate, or phenolate residues, from protein backbone carbonyls, or possibly from water or hydroxide. Bidentate carboxyl groups, such as in thermolysin or concanavalin A (Figure 6), are also a possibility. Water molecules are often found in the coordination sphere of biological calcium-binding sites, and a shared water molecule between calcium and manganese is an interesting prospect. Calcium ions range from 6- to 8-coordinate in biological systems and could provide a storage site with a flexible coordination number for water molecules used in the catalytic cycle.

On the basis of the structures discussed earlier, we present in Figure 7 two possibilities for a Ca-binding site in PS II. In the first case (Figure 7a), we consider the model where the scatterers at >3 Å in the EXAFS arise from Ca (or Sr) alone. In this case a single site with multiple Mn–Ca(Sr) interactions is likely, and Ca is shown bridged to two Mn atoms through single O atoms that could be provided by protein residues or water. The second, more likely possibility, in our view, is a model where both Mn–Mn and Mn–Ca(Sr) interactions contribute (Figure 7b). Both a Mn–Ca-bridged structure with bridging oxygen atoms as described earlier and a Mn–Mn-bridged structure are shown. The Mn–Mn structure would possess an oxo bridge and possibly also one or two bidentate carboxylate bridges (not drawn).

We conclude from this study that the structure of the manganese complex in PS II preparations depleted of Ca and reactivated with Ca is largely unchanged relative to that found in untreated PS II preparations. Reactivation with Sr, however, results in changes in the EXAFS spectra that are consistent with a model in which Ca or Sr ions can occupy a binding site 3.4–3.5 Å from one Mn atom of the manganese complex of PS II. The most likely model based on these data is one in which both Mn–Mn and Mn–Ca interactions give rise to Fourier peak III in the EXAFS collected from these samples. A calcium-binding site at this distance from a metal cluster represents an unusually close association for a biological system and may reflect an intimate role for calcium in water oxidation.

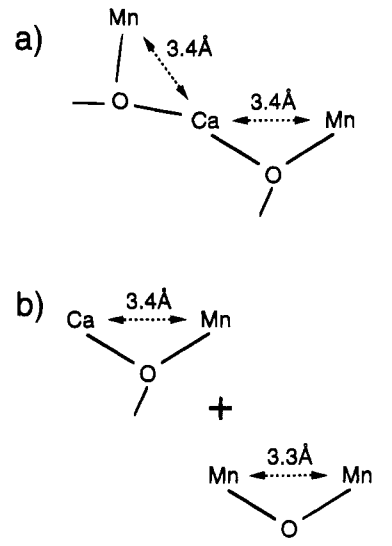

FIGURE 7: Possible structural arrangements for the Ca-binding site in PS II. The bridging structure in (a) corresponds to a model where Fourier peak III is due to only Ca (or Sr) scatterers. The structure depicted in (b) corresponds to a model where both Mn–Ca and Mn–Mn interactions contribute to peak III. In each case, additional bridges may be present, including bidentate and unidentate carboxylates as well as water, hydroxide, phenolate, etc.

ACKNOWLEDGMENT

We thank Dr. Britton Chance for the use of his Ge detector. We are also grateful to Dr. B. Hedman and Dr. S. Khalid for assistance at the beamlines. We thank Joy Andrews, Roehl Cinco, Holger Dau, Melissa Grush, Wenchuan Liang, and Theo Roelofs for help with data collection. We also thank Dr. Jean-Luc Zimmermann for helpful discussions and for assistance with data collection. Synchrotron radiation facilities were provided by the Stanford Synchrotron Radiation Laboratory and the National Synchrotron Light Source, both supported by the DOE. The Biotechnology Laboratory at SSRL and beamline X9-A at NSLS are supported by the National Center for Research Resources of the National Institutes of Health.

REFERENCES

Arnon, D. I. (1949) *Plant Physiol. 24*, 1–15.

Berthold, D. A., Babcock, G. T., & Yocum, C. F. (1981) *FEBS Lett. 134*, 231–234.

Binsted, N., Strange, R. W., & Hasnain, S. S. (1992) *Biochemistry 31*, 12117–12125.

Bonadies, J. A., Maroney, M. J., & Pecoraro, V. L. (1989) *Inorg. Chem. 28*, 2044–2051.

Boussac, A., & Rutherford, A. W. (1988a) *Chem. Scr. 28A*, 123–126.

Boussac, A., & Rutherford, A. W. (1988b) *Biochemistry 27*, 3476–3483.

Boussac, A., Zimmerman, J.-L., & Rutherford, A. W. (1989) *Biochemistry 28*, 8984–8989.

Britt, R. D., Zimmermann, J.-L., Sauer, K., & Klein, M. P. (1989) *J. Am. Chem. Soc. 111*, 3522–3532.

Bunker, G., Bunker, B. A., Crozier, D., Goulon, J., Gurman, S. J., Hasnain, S. S., Heald, S. M., Koningsberger, D. C., Natoli, R., Rehr, J. J., Sayers, D. E., & Udagawa, Y. (1991) *X-ray Absorption Fine Structure* (Hasnain, S. S., Ed.) pp 751–770, Ellis Horwood Ltd., Chichester, U.K.

Cramer, S. P. (1988) in *X-ray Absorption: Principles, Applications, and Techniques of EXAFS, SEXAFS, and XANES* (Koningsberger, D. C., & Prins, R., Eds.) pp 257−320, Wiley-Interscience, New York.
Cramer, S. P., Tench, O., Yocum, M., & George, G. N. (1988) *Nucl. Instrum. Methods Phys. Res. A266*, 586−591.
Dau, H., Andrews, J. C., Roelofs, T. A., Latimer, M. J., Liang, W., Yachandra, V. K., Sauer, K., & Klein, M. P. (1995) *Biochemistry 34*, 5274−5287.
Debus, R. J. (1992) *Biochim. Biophys. Acta 1102*, 269−352.
DeRose, V. J. (1990) Ph.D. Dissertation, University of California, Berkeley, CA (Lawrence Berkeley Laboratory Report LBL-30077).
DeRose, V. J., Mukerji, I., Latimer, M. J., Yachandra, V. K., Sauer, K., & Klein, M. P. (1994) *J. Am. Chem. Soc. 116*, 5239−5249.
Edelman, G. M., Cunningham, B. A., Reeke, G. N., Becker, J. W., Waxdal, M. J., & Wang, J. L. (1972) *Proc. Natl. Acad. Sci. U.S.A. 69*, 2580−2584.
George, G. N., Prince, R. C., & Cramer, S. P. (1989) *Science 243*, 789−791.
Ghanotakis, D. F., Babcock, G. T., & Yocum, C. F. (1984) *FEBS Lett. 167*, 127−130.
Glusker, J. P., Minkin, J. A., & Casciato, C. A. (1971) *Acta Crystallogr. B27*, 1284−1293.
Goodin, D. B., Falk, K.-E., Wydrzynski, T., & Klein, M. P. (1979) *6th Annual Stanford Synchrotron Radiation Laboratory Users Group Meeting*, SSRL Report No. 79/05, pp 10−11, Stanford University, Stanford, CA.
Guiles, R. D., Zimmerman, J.-L., McDermott, A. E., Yachandra, V. K., Cole, J. L., Dexheimer, S. L., Britt, R. D., Wieghardt, K., Bossek, U., Sauer, K., & Klein, M. P. (1990) *Biochemistry 29*, 471−485.
Hardman, K. D., & Ainsworth, C. F. (1972) *Biochemistry 11*, 4910−4919.
Jaklevic, J., Kirby, J. A., Klein, M. P., Robertson, A. S., Brown, G., & Eisenberger, P. (1977) *Solid State Commun. 23*, 679−682.
Kok, B., Forbush, B., & McGloin, M. (1970) *Photochem. Photobiol. 11*, 457−475.
Liang, W., Latimer, M. J., Dau, H., Roelofs, T. A., Yachandra, V. K., Sauer, K., & Klein, M. P. (1994) *Biochemistry 33*, 4923−4932.
Lockett, C. J., Demetriou, C., Bowden, S. J., & Nugent, J. H. A. (1990) *Biochim. Biophys. Acta 1016*, 213−218.
MacLachlan, D. J., Hallahan, B. J., Ruffle, S. V., Nugent, J. H. A., Evans, M. C. W., Strange, R. W., & Hasnain, S. S. (1992) *Biochem. J. 285*, 569−576.
Matthews, B. W., Weaver, L. H., & Kester, W. R. (1974) *J. Biol. Chem. 249*, 8030−8044.
McKale, A. G., Veal, B. W., Paulikas, A. P., Chan, S.-K., & Knapp, G. S. (1988) *J. Am Chem Soc. 110*, 3763−3768.
Mukerji, I., Andrews, J. C., DeRose, V. J., Latimer, M. J., Yachandra, V. K., Sauer, K., & Klein, M. P. (1994) *Biochemistry 33*, 9712−9721.
O'Day, P. A., Rehr, J. J., Zabinsky, S. I., & Brown, G. E., Jr. (1994) *J. Am. Chem. Soc. 116*, 2938−2949.
Ono, T., & Inoue, Y. (1988) *FEBS Lett. 227*, 147−152.
Ono, T., & Inoue, Y. (1989) *Arch. Biochem. Biophys. 275*, 440−448.
Pecoraro, V. L. (1992) in *Manganese Redox Enzymes* (Pecoraro, V. L., Ed.) pp 197−231, VCH Publishers, New York.
Penner-Hahn, J. E., Fronko, R. M., Pecoraro, V. L., Yocum, C. F., Betts, S. D., & Bowlby, N. R. (1990) *J. Am. Chem. Soc. 112*, 2549−2557.
Rehr, J. J., Mustre de Leon, J., Zabinsky, S. I., & Albers, R. C. (1991) *J. Am. Chem. Soc. 113*, 5135−5140.
Rehr, J. J., Albers, R. C., & Zabinsky, S. I. (1992) *Phys. Rev. Lett. 69*, 3397−3400.
Rutherford, A. W., Zimmermann, J.-L., & Boussac, A. (1992) in *The Photosystems: Structure, Function, and Molecular Biology* (Barber, J., Ed.) pp 179−229, Elsevier B. V., Amsterdam.
Sauer, K., Yachandra, V. K., Britt, R. D., & Klein, M. P. (1992) in *Manganese Redox Enzymes* (Pecoraro, V. L., Ed.) pp 141−175, VCH Publishers, New York.
Scott, R. A. (1985) *Methods Enzymol. 117*, 414−459.
Scott, R. A., & Eidsness, M. K. (1988) *Comments Inorg. Chem. 7*, 235−267.
Sheats, J. E., Czernuszewicz, R. S., Dismukes, G. C., Rheingold, A. L., Petrouleas, V., Stubbe, J., Armstrong, W. H., Beer, R. H., & Lippard, S. J. (1987) *J. Am. Chem. Soc. 109*, 1435−1444.
Sivaraja, M., Tso, J., & Dismukes, G. C. (1989) *Biochemistry 28*, 9459−9464.
Teo, B.-K. (1986) *EXAFS: Basic Principles and Data Analysis*, Springer-Verlag, New York.
Tso, J., Sivaraja, M., & Dismukes, G. C. (1991) *Biochemistry 30*, 4734−4739.
Wieghardt, K. (1989) *Angew. Chem., Int. Ed. Engl. 28*, 1153−1172.
Wieghardt, K. (1994) *Angew. Chem., Int. Ed. Engl. 33*, 725−728.
Wieghardt, K., Bossek, U., Ventur, D., & Weiss, J. (1985) *J. Chem. Soc., Chem. Commun.*, 347−349.
Yachandra, V. K. (1995) *Methods Enzymol. 246*, 638−675.
Yachandra, V. K., DeRose, V. J., Latimer, M. J., Mukerji, I., Sauer, K., & Klein, M. P. (1993) *Science 260*, 675−679.
Yocum, C. F. (1991) *Biochim. Biophys. Acta 1059*, 1−15.
Zhang, K., Stern, E. A., Ellis, F., Sanders-Loehr, J., & Shiemke, A. K. (1988) *Biochemistry 27*, 7470−7479.
Zimmermann, J.-L., & Rutherford, A. W. (1986) *Biochemistry 25*, 4609−4615.

BI950989F